Renewable Energy 238 (2025) 121916

Contents lists available at ScienceDirect

Renewable Energy

journal homepage: www.elsevier.com/locate/renene

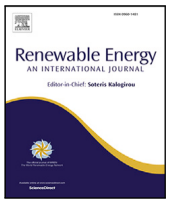

Hydrokinetic energy applications within hydropower tailrace channels: Implications, siting, and U.S. potential

Chien-Yung Tseng [a,c], Mirko Musa [b,c,*]

[a] Department of Civil and Environmental Engineering, Colorado State University, 1372 Campus Delivery, Fort Collins, 80523, CO, USA
[b] School of Architecture, Civil and Environmental Engineering, École Polytechnique Fédérale de Lausanne (EPFL), Lausanne, 1015, Switzerland
[c] Environmental Sciences Division, Oak Ridge National Laboratory, 1 Bethel Valley Rd, Oak Ridge, 37830, TN, USA

ARTICLE INFO

Keywords:
Hydrokinetic energy
Hydropower tailrace
Backwater effect
Optimal siting
Power potential
Analytical model

ABSTRACT

Hydropower tailrace channels are unique and attractive locations for hydrokinetic energy harvesting due to fast currents, scheduled flow releases, proximity to existing structural and electrical infrastructures, and low risk of additional environmental impacts. However, energy-extracting devices create flow resistance, inducing a small but measurable water level increase which may diminish the available hydraulic head and reduce hydropower generation, defeating the initial value proposition. This study combines a one-dimensional momentum balance approach with the backwater equation for surface-varying open channel flow to analyze the water level increase and determine the optimal turbine siting distance that maximizes the net power production (balancing hydropower loss vs. hydrokinetic gain), as a function of the channel hydraulic conditions and the hydrokinetic turbine characteristics. Finally, using a subset of sites from the U.S. hydropower fleet, we provide a high-level estimation of the hydrokinetic potential available in tailraces in the United States and discuss two case studies. This work advocates for the adoption of hydrokinetic turbines downstream of dams as an opportunity to increase energy production at existing plants and Non-Powered Dams (NPDs) with minimal structural intervention, and, alternatively, as viable sites for large-scale field testing for hydrokinetic devices.

1. Introduction

In recent years, renewable energy has been the primary driver of energy growth in the United States. According to the U.S. Energy Information Administration (EIA), electricity generation from renewable sources exceeded generation from nuclear in 2021 and for the first time from coal in April 2022 [1], providing 24% of total U.S. electricity generation in the first six months that year [2]. The rise of renewables has largely stemmed from state and federal government policies and financial incentives, gaining further momentum as communities and governments continue their efforts to "transition away from fossil fuels" [3].

Although wind has recently become the largest source of renewable energy generation in the country, hydropower has been contributing to clean and renewable energy for over a century [4]. In 2022, it accounted for 28% of all the renewables and 6% of the total energy production in the U.S. [5]. Conventional hydropower captures the potential energy of a hydraulic head by forcing the water through pressurized water conveyances connected to highly efficient hydraulic turbines. In contrast, marine and riverine hydrokinetic technologies capture the kinetic energy available in free-flowing water using Current Energy Converters (CEC) technologies [6–8], which resemble wind turbines in both geometry and working principle [9]. Whilst conventional hydropower is still the largest source of energy from water, hydrokinetic energy remains widely undeveloped, with vast untapped power potential in U.S. [10] and worldwide [11,12]. Significant interest and research has recently focused on accelerating hydrokinetic technology development [13–18, among many others] and deployment [19–24, among many others]. In particular, inland hydrokinetic applications in rivers and man-made canals have recently garnered interest [12, 25–28] due to their relatively simple installation and maintenance compared to marine deployments. Examples of such deployments are emerging in the United States in recent years. For instance, the company Emrgy Inc. [29] developed modular vertical-axis turbines for artificial canals which they have recently started deploying across the U.S. Another prominent example is Ocean Renewable Power Company (ORPC) which installed and operates riverine cross-flow horizontal axis devices in Igiugig, Alaska [30] and has recently received additional funding from the U.S. Department of Energy (DOE) to deploy two new

* Corresponding author at: School of Architecture, Civil and Environmental Engineering, École Polytechnique Fédérale de Lausanne (EPFL), Lausanne, 1015, Switzerland.
E-mail address: mirko.musa@epfl.ch (M. Musa).

https://doi.org/10.1016/j.renene.2024.121916
Received 26 March 2024; Received in revised form 29 October 2024; Accepted 14 November 2024
Available online 23 November 2024

tidal energy devices [31]. Riverine and canals deployments can offer a promising avenue for distributed renewable energy in remote and rural regions [32–34] and are also perceived as complementary to traditional hydropower with less environmental footprint [35]. However, systemic environmental impacts need to be fully considered and site selections can significantly dictate project feasibility. As such, opportunities to streamline project development and reduce barriers to licensing could be realized via thoughtful site selections, potentially through collaborations with local communities [31,33]. One potential deployment paradigm that could expedite project approval is the installation of hydrokinetic turbines within tailrace channels downstream of hydropower facilities, which represents a unique and attractive subset of potential CEC riverine applications [36].

1.1. Hydropower tailrace channels: advantages and challenges for hydrokinetic energy development

Hydropower tailrace channels have several advantages for CECs installation: (i) high-velocity currents and thus hydrokinetic energy potential, (ii) regulated predictable flow releases, and (iii) proximity to existing electrical interconnections and engineered structures (to serve as mooring, anchorage, or foundation). From an environmental perspective, tailrace channel applications may also entail minimal new environmental impacts as most of the alterations have already occurred during the hydropower development, potentially expediting the licensing process. CECs and other water wheel applications [37] have relatively low civil work requirements and costs, which are easily scalable and can potentially provide ancillary services.

Although hydrokinetic turbine deployment in hydropower tailrace channels remains largely unexplored in both academic research and commercial development, a few studies have previously examined this opportunity. For example, Lalander and Leijon [38] used analytical and numerical models to study the impact of in-stream hydrokinetic energy converters on the upstream water level in a channel downstream of a hydropower plant in east Sweden. Liu and Packey [39] discussed the challenges and advantages associated with a "combined-cycle hydropower system (CCHS)", which integrates hydrokinetic turbines downstream of hydropower stations, focusing on the technical, economic, and environmental implications. Ramírez et al. [40] performed a pre-feasibility technical and financial evaluation of a hydrokinetic energy project at two large hydropower facilities in Colombia. Holanda et al. [41] conducted river hydrodynamic modeling to analyze the velocities and depths in a channel downstream of the UHE Tucuruíhydropower plant on the Tocantins River in Brazil to estimate the hydrokinetic potential. They also provided a valuable literature review on hydrodynamic models and other tailrace hydrokinetic application studies. Finally, Ladokun et al. [42] assessed the potential and feasibility of installing hydrokinetic turbines behind three major hydropower dams in Nigeria.

Nonetheless, in addition to challenges common to most modern CEC systems, such as low technology readiness levels, high levelized cost of energy (LCOE), and environmental uncertainties, tailrace applications may negatively impact the upstream hydropower facility's performance. This potential interference with hydropower generation is a primary concern among stakeholders, in addition to the added operational constraints that a tailrace CEC deployment could introduce — a topic that remains under-researched.

Within a hydropower reservoir system, the power produced by the turbine(s) is directly proportional to the hydraulic head (i.e., the difference between upstream and downstream water levels) and the flow rate passing through the turbine(s), as illustrated by the power equation:

$$P = \gamma \eta Q H \tag{1}$$

where P is the power capacity, γ is the specific weight of water, Q is the discharge rate (or flow) of water, H is the hydraulic head, and η is the overall efficiency of the hydropower plant, which includes turbine efficiency — typically around 85%–90% for most modern hydropower turbine units. The flow resistance induced by CEC devices downstream of the dam could undermine the available head by causing a small but measurable water level increase in the tailrace channel. In subcritical flow conditions (i.e., Froude numbers, Fr, lower than 1), in fact, any blockage in the flow has the potential to induce a backwater effect (i.e., an increase in water level immediately upstream of the blockage). The Froude number assesses the relative significance of flow inertia to that of the gravitational force and is defined as $Fr = V/\sqrt{gh}$, where V is the water velocity, g is the gravitational acceleration, and h is the water flow depth. Depending on the distance between the devices and the upstream hydropower facility, the water increase can diminish the available hydraulic head and production of the hydropower facility, offsetting a portion of the benefits of CEC deployment and production.

Existing literature [38,43–45] have shown that the extent of the backwater effect depends on numerous factors, most importantly, the scale of the CEC deployment (e.g., unit configuration and associated flow blockage). However, none of these studies (to the best knowledge of the authors) have directly linked these effects to the potential hydropower losses or discussed the optimal hydrokinetic siting to minimize these losses and maximize the net power generation. Hydropower losses can in fact be avoided by installing the hydrokinetic devices further downstream, at a distance where the backwater has recovered to the upstream undisturbed level [38,45], yielding a research direction to investigate the favorable siting locations under different CEC device characteristics and hydrodynamic scenarios. Therefore, in this study we introduce a simplified one-dimensional momentum balance model, coupled with the backwater equation, to represent variable surface conditions in tailrace channel flow. This model enables an analytical assessment of potential hydraulic head loss due to CEC turbine installation in hydropower tailrace channels and, for the first time, explores optimal siting strategies to minimize — or even avoid — the impact of head loss on net power production. This work examines how channel hydraulic conditions and CEC device characteristics affect the necessary downstream siting distance to ensure positive net power production from the CEC–hydropower combined system. This approach offers a tractable method for estimating hydraulic and power effects across a range of potential applications, with opportunities for further refinement in future research.

The paper is organized as follows. In Section 2, we present the theoretical framework of the 1D momentum conservation model along with the surface-varying backwater equation to estimate backwater rises, surface water elevation profiles, and net power generations from the system. In Section 3, we show the model results of backwater rise and compare them with previous experimental/field/numerical data for validation. In Section 4, we discuss the net power generation according to different CECs siting locations under different channel hydraulic conditions and CEC device characteristics. Lastly, in Section 5, we provide a high-level estimation of the potential power resources from hydropower tailrace channels in the United States and discuss two example sites from the U.S. hydropower fleet to conduct potential case studies where the proposed models, in tandem with additional preliminary assessments, can be applied to evaluate potential field demonstration projects.

2. Theoretical framework

2.1. Momentum conservation and backwater rise

The simplified one-dimensional (1D) momentum analysis is presented herein to evaluate CEC tailrace application by exploring concepts from existing literature [e.g.,38,39] and is inspired by Kartezhnikov and Ravens [43] and Cacciali et al. [46] who estimated the hydraulic responses associated with the CEC presence by considering the energy conservation equation (or modified Bernoulli equation) in

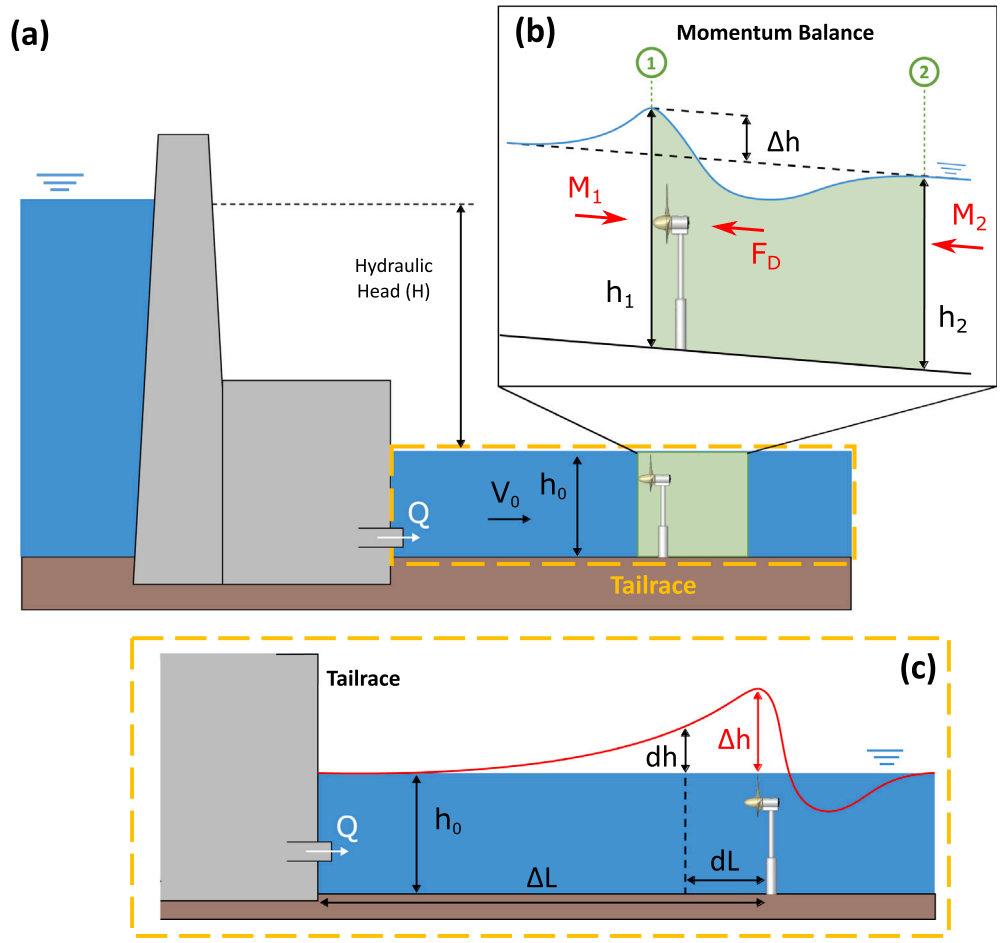

Fig. 1. (a) Schematic of an example hydropower dam system and free-flowing tailrace, with undisturbed velocity and water depth conditions (i.e., V_0 and h_0). Not to scale. (b) Schematic of the control volume for the one-dimensional momentum balance approach used in this study, with M being the hydraulic forces acting on cross-sections 1 and 2 (vertical green lines), and F_D being the drag force exerted by the CEC turbine. (c) A zoom-in schematic of the tailrace region to illustrate the backwater increase by the CEC turbine and the resulting water surface profile denoted by the red curve. Δh is the maximum water level increase at CEC's location. dh is the water level increase at the incremental distance, dL, upstream from the CEC. ΔL is the total distance between the CEC and the dam. In the case shown above, ΔL is the same as the distance required for the surface water level to fully recover back to normal, that is $\Delta L = \Delta L_n$.

the channel. The analysis proposed here focuses on the momentum conservation [44], including further considerations of net power production across a relatively narrow, yet physically representative, range of nondimensional input parameters. Two fundamental simplifying assumptions were made in the analysis. First, the CEC power generation and hydropower loss were linked, assuming that the flow released by the powerhouse was the only flow in the channel available to the CEC turbines (i.e., no spillway flow). Second, the tailrace channel was assumed ideally rectangular, and the flow was homogeneous in the channel.

A schematic of the 1D analytical setup is provided in Fig. 1. Herein, the hydropower–dam–tailrace system without CECs is referred to as the "undisturbed" case, and the modified system with CECs deployment as the "disturbed" case.

The presence of CECs in the tailrace channel introduces significant energy dissipation and exerts an additional drag on the flow, which elevates the upstream water level [38,43,44,46]. To estimate this backwater effect, a simple 1D momentum balance approach was applied (see the control volume shown in Fig. 1b). Specifically, cross-section 1 of the control volume is selected at the turbine rotor location, where h_1 is the maximum water depth increase resulting from the CEC presence. Cross-section 2 is located far enough downstream, at a point where the flow has recovered to the undisturbed conditions. The length of this recovery is dictated by several factors controlling the entrainment and mixing of high-momentum flow surrounding the wake (e.g., turbine geometry and operations, incoming flow velocity and turbulence intensity, boundary effects, etc.), and it is normally expressed in terms of turbine rotor diameters. Wake structures behind turbines have been extensively studied in wind energy research [e.g.,47–52, among many others] and later extended to hydrokinetic turbines. Several experimental measurements [e.g.,20,53–58, among others] and numerical simulations [e.g.,59–64, among others] have proposed different characteristic lengths depending on the percentage of recovery. Recent literature reviews from Nago et al. [65] and Niebuhr [66] have summarized some of these findings, highlighting the need to understand and model wake dissipation for optimizing turbine placement in arrays. Given the analytical nature of the analysis presented herein, rather than specifying an exact physical location, the downstream boundary of the control volume (cross-section 2) is located where wake recovery is achieved.

Fig. 1a shows the undisturbed conditions in the tailrace without CECs. Given the control volume, the change in flow depth can be evaluated by imposing the 1D momentum balance as:

$$M_1 = M_2 + \frac{F_D}{W} \tag{2}$$

where F_D is the drag force exerted by the turbine, W is channel width, and M represents the force per unit width exerted by the flow, which can be expressed as $M = \rho V^2 h + \rho g \frac{h^2}{2}$ with V being the flow velocity and h being the water depth. Hence, Eq. (2) can be expressed as

$$\rho V_1^2 h_1 + \rho g \frac{h_1^2}{2} = V_2^2 h_2 + \rho g \frac{h_2^2}{2} + F_D/W \tag{3}$$

Dividing by the specific weight of water (i.e., $\gamma = \rho g$) and applying mass continuity, thereby assuming the same flow rate per unit width, q, between cross-section 1 and cross-section 2 (i.e., $q = V_1 h_1 = V_2 h_2 = V_0 h_0$, where V_0 and h_0 are the undisturbed flow conditions, Fig. 1a), Eq. (3) can be rewritten as:

$$\frac{q^2}{g h_1} + \frac{h_1^2}{2} = \frac{q^2}{g h_2} + \frac{h_2^2}{2} + \frac{F_D}{\gamma W} \tag{4}$$

As mentioned previously, cross-section 2 is assumed to be located far enough downstream of the CEC turbine such that the water depth and flow velocity have recovered to the undisturbed conditions (i.e., $h_2 = h_0$ and $V_2 = V_0$, Fig. 1a). Rearranging terms in Eq. (4) leads to the following expression:

$$\left(\frac{h_1}{h_0}\right)^3 - 2\left(Fr_0^2 + \frac{1}{2} + \frac{F_D}{\gamma W h_0^2}\right)\left(\frac{h_1}{h_0}\right) + 2Fr_0^2 = 0 \tag{5}$$

where $Fr_0^2 = V_0/\sqrt{g h_0}$ is the Froude number in the undisturbed conditions.

As flowing water impacts an operating CEC turbine, the turbine exerts an equal and opposing drag force, which can be dimensionally expressed as the total power of the flow dissipated by the device divided by the incoming velocity (which in cross-section 1 is equal to V_1). In other words, this power is the work of the drag force acting on the turbine against the flow. This dimensional argument was used by Manes and Brocchini [67] to develop an analytical predictive model for bridge pier scour (based on scaling arguments first introduced by Gioia and Bombardelli [68]) and by Musa et al. [69] for hydrokinetic turbine scour. This representation of the drag force is also at the base of hydrodynamic model simulations used for resource assessment and environmental impact evaluation [70–73]. Therefore, the total drag force exerted by an operating CEC can be expressed as:

$$F_D = \frac{P_{diss}}{V_1} \tag{6}$$

where P_{diss} is the total power dissipated in a channel by the CEC turbine. This term includes both the power extracted by the turbine (P_{CEC}), as a result of the kinetic energy conversion into mechanical energy, and the additional loss due to the turbulent mixing occurring in the wake of the turbine. Note that this formulation ignores the drag losses due to the support structure (base and tower) deemed negligible if compared to the operating rotor. Garrett and Cummins [74] analytically observed that for ideal turbines operating near the maximum theoretical efficiency limit (the Lanchester–Betz limit), the ratio between the power extracted and the total power dissipated can be approximated as:

$$\frac{P_{CEC}}{P_{diss}} = \frac{2}{3(1+\epsilon)} \tag{7}$$

where ϵ is the flow-blockage ratio coefficient (i.e., the ratio between the turbine rotor's cross-swept area and the cross-sectional area of the channel). Polagye [75] demonstrated that Eq. (7) is only applicable under certain conditions (i.e., small blockage ratios, $\epsilon < 0.2$, and low Froude numbers, $Fr < 0.4$), extending the relation to less restrictive assumptions. However, Polagye's comprehensive analysis led to a more complicated relation between total power dissipation and boundary conditions, requiring numerical solutions for a complete characterization. Therefore, for the scope of the current study, the simplified approach by Garrett and Cummins [74] is adopted, and their assumptions and limitations are acknowledged for the corresponding parameter setups (see Section 3).

Similar to wind turbines [76,77], the power extracted by a CEC turbine can be expressed as:

$$P_{CEC} = \frac{1}{2}\rho c_P A_T V_1^3 \tag{8}$$

where ρ is the density of water, c_P is the CEC turbine efficiency, and A_T is the area swept by the turbine rotor blades. The CEC turbine efficiency and cross-swept area both relate to the manufacturing specifications of the CEC device.

Combining Eq. (6) with Eqs. (7) and (8), and recalling that the blockage ratio is $\epsilon = A_T/A_{ch_1}$ (where A_{ch_1} is the channel cross-sectional area 1), the drag force expression can be rewritten as

$$F_D = \frac{3}{4}\rho c_P \epsilon A_{ch_1}(1+\epsilon)V_1^2 \tag{9}$$

Substituting Eq. (9) into Eq. (5) and regrouping terms lead to a nondimensional third-order expression for the ratio between the new disturbed and undisturbed water levels:

$$\left(\frac{h_1}{h_0}\right)^3 - 2\left(Fr_0^2 + \frac{1}{2}\right)\left(\frac{h_1}{h_0}\right) + \left(2 - \frac{3}{2}c_P\epsilon(1+\epsilon)\right)Fr_0^2 = 0 \tag{10}$$

Eq. (10) shows that the water level increase induced by the presence of operating CEC turbines (which occurs at the CEC location) ultimately depends on the existing hydraulic conditions (represented by the upstream Froude number, Fr_0^2) and turbine characteristics (the device efficiency, c_P, and the blockage ratio, ϵ). By including only nondimensional parameters, this analysis is generalizable to any CEC-channel configuration. Without turbines (i.e., $c_P = 0$ and $F_D = 0$), the last term in Eq. (10) is eliminated, in which case the resulting expression reduces to the classic equation for the conjugate depth in hydraulic jumps if factorized by $h_1/h_0 - 1 = 0$ (i.e., the trivial solution $h_1 = h_0$), thereby providing support for the equation's form.

2.2. Upstream water level recovery

Another goal of this study is to determine an optimal CEC siting location by considering the recovery of the surface water level so as to ensure a positive net power generation from the combined CEC tailwater hydrokinetic energy and hydropower. Therefore, we apply the classic backwater equation for surface-varying open channel flow:

$$\frac{dh}{dx} = \frac{S - C_f Fr^2}{1 - Fr^2} \tag{11}$$

where S is the channel slope and C_f is the bottom drag coefficient that depends on the bottom roughness of the riverbed. In the tailwater region, the channel is partially mixed with artificially constructed concrete that creates a smoother bed compared to a purely natural rocky riverbed, suggesting small coefficients such as $C_f \approx 0.005$ according to the typical value of Manning's coefficient, $n \approx 0.012$ for fully-concrete channels and $n \approx 0.03$ for natural river channels [78]. The total distance, ΔL_n, required for the surface water level to fully recover back to normal (where $dh/dx = 0$) can be obtained by calculating the integration of Eq. (11) over the maximum water increase Δh at CEC's location (see Fig. 1c):

$$\Delta L_n = \int_0^{\Delta h} \frac{1 - Fr^2}{S - C_f Fr^2}\delta h \tag{12}$$

where $\Delta h = h_1 - h_0$ can be obtained based on Eq. (10). However, since Fr is a function of h, Eq. (12) cannot be solved explicitly. Alternatively, we divided Δh into 100 water elevation change intervals to numerically integrate Eq. (12) by updating h and Fr incrementally to obtain ΔL_n. By summing the intervals, the water elevation increase (dh) profile at the varying upstream distance from the CEC (dL) can be obtained. Fig. 1(c) illustrates the notations (Δh, dh, and dL).

2.3. Net power production

To better understand how the hydraulic conditions of tailrace CECs could affect the upstream hydropower facility and to evaluate the productivity and efficiency of tailrace CECs deployment, the analysis is expanded to evaluate overall net power production (i.e., CEC power production vs. hydropower plant loss). Given a hydropower turbine at a fixed elevation, a water level increase (Δh) in the tailrace channel corresponds to a decrease of the available hydraulic head (H), which leads

to a net loss in power potential (ΔP_H) for the upstream hydropower facility. From Eq. (1) it can be shown that:

$$\Delta P_H = \gamma \eta Q \Delta h \tag{13}$$

In this section, water level increase is analytically linked to the ratio between CEC power production Eq. (8) and hydropower plant loss Eq. (13) by assuming that the tailrace flow Q available for CEC power production consists only of the powerhouse flow discharge. Thus recalling that the hydrokinetic turbine cross-swept area can be expressed in terms of the channel blockage ratio as $A_T = \epsilon A_{ch_1}$ and the flow rate is $Q = V_1 A_{ch_1}$, Eq. (8) is rewritten as:

$$P_{CEC} = \frac{1}{2}\rho c_P \epsilon Q V_1^2 \tag{14}$$

Additionally, using mass continuity (i.e., $q = V_1 h_1 = V_0 h_0$), the velocity V_1 can be expressed as a function of the undisturbed conditions, $V_1 = h_0/h_1 V_0$. Substituting $\Delta h = h_1 - h_0$ and rearranging terms, the ratio between CEC power production Eq. (8) and hydropower plant loss Eq. (13) can be expressed as:

$$\frac{P_{CEC}}{\Delta P_H} = \frac{1}{2}\frac{c_P \epsilon Fr_0^2}{\eta}\frac{1}{h_1/h_0 - 1}\left(\frac{h_0}{h_1}\right)^2 \tag{15}$$

Note that the ratio h_1/h_0 is a function of the other parameters on the right (except for η) through the expression derived in Eq. (10). Therefore, for any set of hydraulic conditions (Fr, here means the initial Froude number, Fr_0) and turbine configuration (c_P and ϵ), the normalized water level increase (h_1/h_0) and the associated gain-to-loss power ratio ($P_{CEC}/\Delta P_H$) can be estimated. Moreover, to ensure the positive net power production (i.e., $P_{CEC}/\Delta P_H > 1$), we can further combine Eq. (15) with Eq. (12) to consider the water surface level recovery upstream from the CECs. Since $h_1/h_0 - 1 = \Delta h/h_0$, where Δh can be numerically integrated as discussed previously in Eq. (12), we thus can estimate the minimal required distance between the dam and the siting location of CECs for $P_{CEC}/\Delta P_H > 1$. Given this study's scope and purpose, the key exploratory concept was to assess how different combinations of CECs designs (c_P and ϵ) and hydraulic conditions (Fr) will affect the net power production and the required distance for the CECs siting locations. Detailed discussions are presented in Section 4.

3. Validation and model sensitivity

3.1. Validation

Direct measurement of backwater effects induced by operating a hydrokinetic turbine is not typically one of the main parameters monitored in experimental studies and only a handful of examples exist (to the knowledge of the authors). Examples of these observations can be found in [53,79–82]. To validate our simplified analytical model, results were compared against three sources of backwater measurements at three different scales [54,79,83] and one numerical simulation [43].

Chamorro et al. [54] and Hill et al. [79] reported experiments conducted at the St. Anthony Falls Laboratory of the University of Minnesota using two scales of the same turbine model design (0.5 m and 0.15 m rotor diameter, respectively) and two different channels (Main Channel – 85 m long and 2.75 m wide, and the Tilting Bed Flume – 15 m long and 0.9 m wide). The experiments underwent peer review; however, the water surface elevation (w.s.e.) data depicted in Fig. 2 and used for our validation were not included in the published work but were acquired through private communication with the authors. All the experimental setups and methods can be found in the cited references. The main relevant parameters to our study are summarized in Table 1. For both experiments, the w.s.e. was measured using Massa M5000 ultrasonic sensors but with different techniques. Data from Fig. 2a were collected using stationary Massa sensors in different locations along the channel; black lines with symbols represent different spanwise (y) transects, while the blue line represents their average. For data from Fig. 2b, a Massa sensor was installed on an automated data acquisition carriage capable of traversing the entire length of the flume while simultaneously acquiring measurements. The w.s.e data was recorded at 5 mm increments (hence the higher resolution in the plot) along the flume streamwise centerline repeatedly for the entire duration of the experiment. The blue solid line represents the time-averaged data. In both cases, w.s.e profiles were detrended subtracting their average slope. The detrended value of the w.s.e at the turbine location was used as the best estimate for the maximum water increase, Δh. To mitigate the uncertainties associated with the signal (and water) waviness in Fig. 2b, the interpolation of the upstream section (red line) was used [79].

The third set of measurements was collected by Gunawan et al. [83,84] during field tests of a full-scale turbine deployed in a man-made canal. The field measurement campaign was conducted in 2014 at Roza Canal, Yakima, WA, where a 25 kW 3-blade vertical-axis Darrieus turbine (3 m wide and 1.5 m high) was deployed and tested for two years. Measurements included water level and velocity upstream and downstream of the device, as well as turbine performance. Most of the parameters needed for our validation (Froude number Fr, undisturbed flow depth h_0, turbine blockage ratio, ϵ, and most importantly, the water increase Δh) were reported in Gunawan et al. [83,84] and are listed in Table 1. Conversely, the turbine's power coefficient c_P was not published, as it is typically proprietary information. Hence, we assumed a typical value for vertical-axis turbines as reported in the literature for similar Reynolds numbers (see, for instance, Bachant and Wosnik [85] and Strom et al. [86] for water turbines, or Miller et al. [87] for wind turbines).

In addition, we compared our model results to the 1D analytical model proposed by Kartezhnikova and Ravens [43]. Their model estimated the hydraulic impacts of hydrokinetic devices by using an enhanced Manning's (bottom roughness) coefficient, which considered energy balance in the governing equations to estimate the hydraulic impacts, including responses on water elevation. They further combined the analytical model with a 2D numerical model to illustrate the estimation of the deployment of hydrokinetic devices on a field scale.

The comparisons between our modeled water level increase and the measured values in the previous lab experiments, field survey, and numerical model across different scales are presented in Table 1. The results obtained from our simplified analytical model show a fairly good agreement with the measured data, thus providing validation for our approach.

3.2. Backwater effect

Given the simplifying assumptions of the approach presented in Section 2, the backwater effect and net power production were evaluated across a relatively narrow yet physically representative range of input parameters. The simple analysis presented herein was applied for CEC turbine(s) installed in a single cross-section of an open channel (i.e., the tailrace). Rather than specifying physical turbine dimensions and unit count, the total blockage ratio, defined as the ratio between the total frontal area of the device(s) and the channel cross-section, was prescribed.

Fig. 3 shows the percent increase in flow depth (i.e., % of $\Delta h/h_0$ or % of $h_1/h_0 - 1$) resulting from tailrace CEC deployment across various variables of (a) blockage ratio (ϵ), (b) Froude number (Fr), and (c) CEC power coefficient (c_P). To show the dependence of the water increase on each individual parameter, the other two parameters were fixed. Specifically, $Fr = 0.13$, $\epsilon = 5\%$, and $c_P = 45\%$ were selected as fixed values for demonstration. As a dimensional example, for a hypothetical 150 m wide tailrace channel with an undisturbed depth of 6 m, the selected blockage ratio would be representative of a row of six, 3 m diameter CEC turbines, whereas the Froude number would correspond to an incoming flow velocity of $V_0 = 1$ m/s for the 6 m flow depth. The selected power coefficient, considered at optimal tip–speed

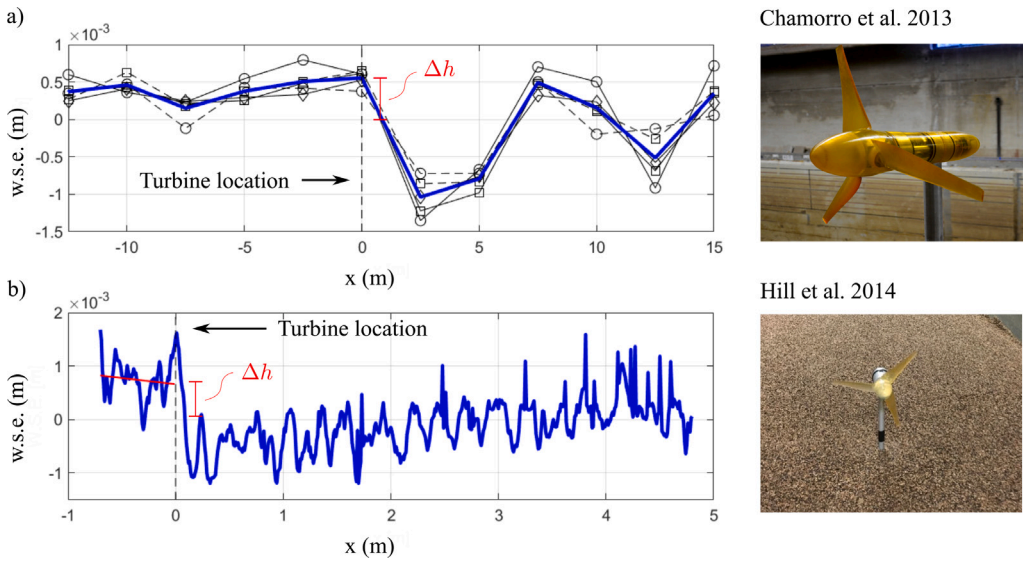

Fig. 2. (a) w.s.e. measurements by Chamorro et al. [54], detrended from the average slope; black lines with symbols represent measurements at different spanwise locations, and blue solid line is their average. (b) w.s.e. measurements by Hill et al. [79]; the blue solid line shows the time-averaged free surface, and the solid red line represents the upstream linear trend. In both plots, Δh is the estimated maximum water increase.

Table 1
Water level increase, Δh, measured (green) and modeled using Eq. (10) (blue) with the corresponding hydraulic conditions and CEC parameters from previous studies: scale, undisturbed flow depth h_0, undisturbed Froude number Fr_0, blockage ratio ϵ, and power coefficient c_P.

	Hill et al. [79]	Chamorro et al. [54]	Gunawan et al. [83]	Kartezhnikova & Ravens [43]
Test Type	Laboratory experiment	Laboratory experiment	Field monitoring	2D numerical simulation
Flow depth (h_0)	0.28 m	1.15 m	3.3 m	10 m
Froude Number (Fr_0)	0.27	0.12	0.4	0.263
Blockage Ratio (ϵ)	7.2%	6.2%	16%	17.25%
Power coefficient (c_P)	0.4 (estimated)	0.45	0.25 (assumed)	0.32
Water increase Δh **measured**	0.0007 m $\Delta h/h_0$ = 0.25%	0.0006 m $\Delta h/h_0$ = 0.05%	0.030 m $\Delta h/h_0$ = 0.91%	0.057 m $\Delta h/h_0$ = 0.56%
Water increase Δh **modeled**	0.0005 m $\Delta h/h_0$ = 0.18%	0.0004 m $\Delta h/h_0$ = 0.03%	0.022 m $\Delta h/h_0$ = 0.66%	0.036 m $\Delta h/h_0$ = 0.36%

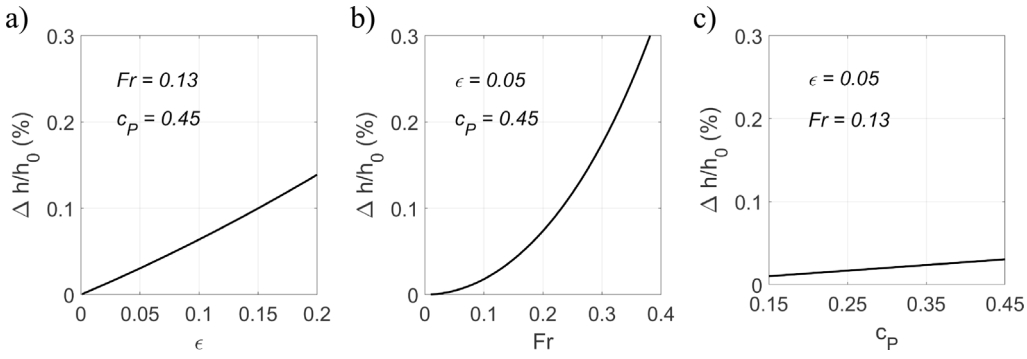

Fig. 3. Percent change in flow depth, $\Delta h/h_0$ (%), as function of (a) blockage ratio ϵ with fixed $Fr = 0.13$ and $c_P = 45\%$; (b) Froude number Fr with fixed $\epsilon = 5\%$ and $c_P = 45\%$; and (c) CEC turbine efficiency c_P with fixed $Fr = 0.13$ and $\epsilon = 5\%$.

ratio (i.e., peak performance), represents a fairly high but reasonable efficiency coefficient for modern CEC technologies, as reported in the literature [9,88]. Specifically, $c_P = 0.45$ was chosen here to reflect the performance of the turbine model measured in a laboratory setting by [54], which was used for our validation in Section 3.1. The ranges of blockage ratio and Froude number included in Fig. 3 were selected to be consistent with the underlying assumption of the specific range of small ϵ and Fr in Eq. (7).

The results shown in Fig. 3 confirm that installing CEC turbines within a hydropower tailrace will result in an increased water surface elevation whose magnitude increases as any of the parameters (blockage ratio, Froude number, and CEC turbine efficiency) increase. Within

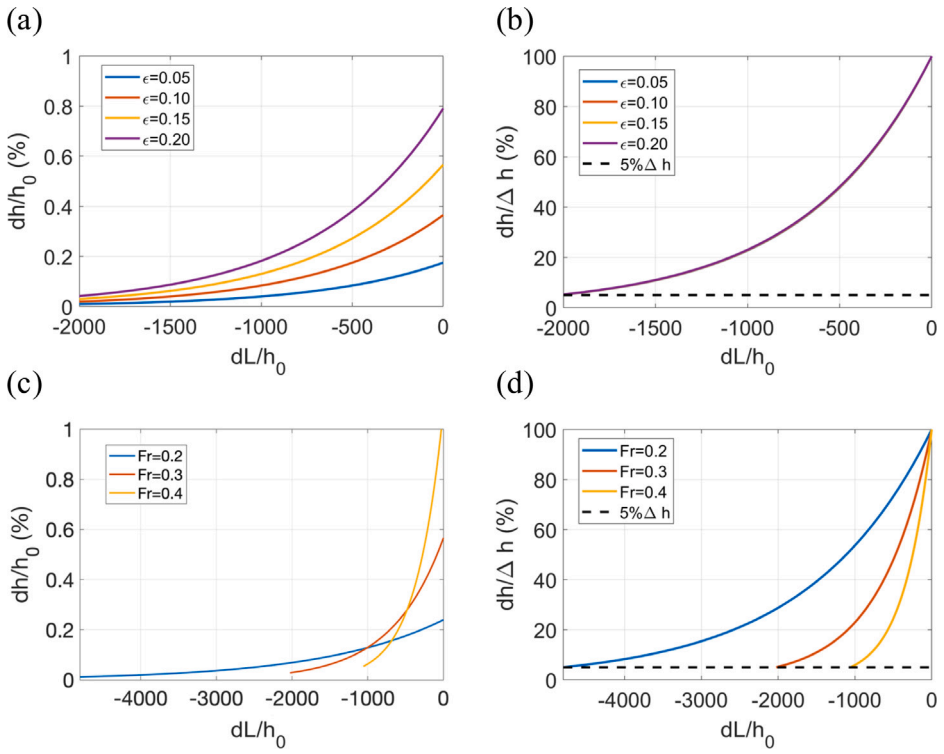

Fig. 4. Recovery profile of surface water elevation (a) and (b) with fixed $c_P = 45\%$, $Fr = 0.3$ (corresponding to $S = 0.0005$ for an equilibrium open channel flow, where S is the channel slope), and varying $\epsilon = 5\%$,10%,15%, and 20%; (c) and (d) with fixed $c_P = 45\%$ and $\epsilon = 15\%$, and varying $Fr = 0.2$, 0.3, and 0.4 (corresponding to $S = 0.0002 - 0.0008$). (a) and (c) are profiles normalized by the undisturbed water depth, h_0. (b) and (d) are profiles normalized by the maximum water level increase, Δh. The calculation of the recovery profiles is terminated when dh is within 5% the maximum water level increase Δh.

the selected ranges, both blockage ratio and Froude number show a relatively strong effect with a concave-up, quadratic trend especially for Froude number, whereas an increase in CEC turbine efficiency appeared to have a relatively smaller effect.

3.3. Water level recovery

Given the results presented in Fig. 3, we selected the Froude number and blockage ratio as two study parameters to investigate the recovery curve of the water surface elevation upstream of the CEC location. The recovery profiles shown in Fig. 4 were calculated based on the numerical integration method provided by Eq. (12) under two scenarios: (a) and (b) with fixed Froude number ($Fr = 0.3$) and four different blockage ratios: $\epsilon = 5\%$, 10%, 15%, and 20%; (c) and (d) with fixed blockage ratio ($\epsilon = 15\%$) and three different Froude numbers: $Fr = 0.2$, 0.3, and 0.4. CEC turbine efficiency was set as $c_P = 45\%$ following the previous setup. The notation dh represents the water surface increase induced by the turbine and recovering to the undisturbed uniform flow upstream, and dL represents the corresponding distance upstream from the CEC (refer to the illustrative sketch in Fig. 1c). The recovery profile is calculated numerically solving Eq. (11) and (12). The solution of the recovering water level profile is asymptotic to the uniform flow level. Therefore, to provide a practical location in terms of optimal CEC siting, the calculation is terminated when dh is within 5% the maximum water level increase Δh.

As shown in Figs. 4a and 4b, different blockage ratios cause different maximum water level rises, Δh. However, under the same Froude number, the profiles show similar concave-up curves, which can be observed when the curves are normalized by Δh, as all profiles collapse into one single curve shown in Fig. 4b. This similarity is explained by considering that the blockage ratio is a characteristic of the size of the turbine and does not directly affect the recovery profile equations. Under this condition, higher blockage ratios result in higher rises in water level, necessitating a longer distance upstream of the CECs for the water surface to recover to its undisturbed level.

When fixing the blockage ratio, different Froude numbers would not only cause different Δh, but also result in curves with different trends, as shown in Figs. 4c and 4d. An increase in Froude number corresponds to a higher drag force exerted by the CEC device, thus resulting in a large water surface elevation increase. However, higher Froude numbers also lead to a shorter distance required for the water level to recover to its undisturbed levels upstream of the CEC. This is justified by the presence of the Froude number in both the solution for Δh and in the recovery profile equations. Under the equilibrium (normal flow) condition, the bottom slope, S, determines the Froude number as indicated by Eq. (11), when $dh/dx = 0$, $Fr = \sqrt{S/C_f}$. Therefore, a larger Froude number with fixed bottom roughness represents a steeper slope system (faster flows) which leads to a faster water surface recovery upstream from the CEC. Based on the relation mentioned above, the fixed Fr in Figs. 4a and 4b corresponds to a slope of $S = 0.0005$, while the range $Fr = 0.2 - 0.4$ used in Figs. 4c and 4d corresponds to $S = 0.0002 - 0.0008$.

4. Net power production and turbine siting location

Section 3 shows how water surface level changes with different parameters like c_P, ϵ, and Fr. In this section, we explore how these parameters may affect the net power production according to different CEC siting locations. The net power is defined as the comparison (ratio) between the hydrokinetic energy produced (P_{CEC}) and the potential hydropower generation loss (ΔP_H) induced by the water level increase due to the operating CEC. The backwater effect and the power ratio are linked analytically as shown in Section 2.3.

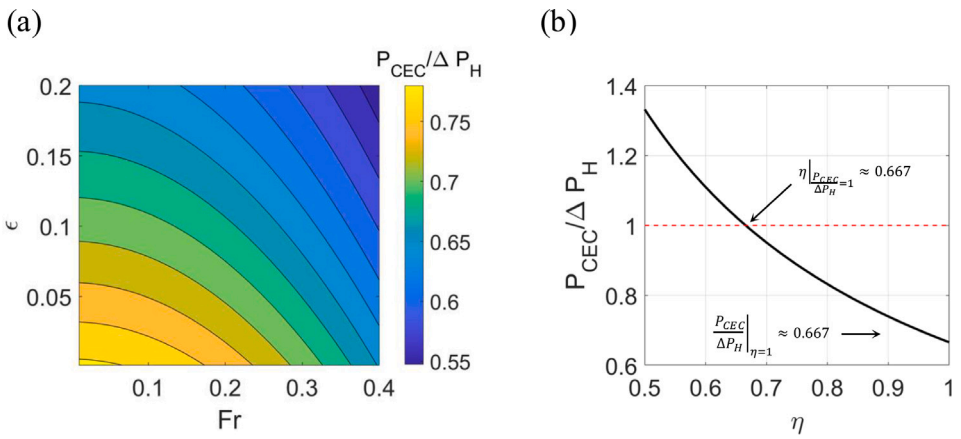

Fig. 5. Power ratio $P_{CEC}/\Delta P_H$ for (a) $c_P = 0.45$, $\eta = 0.85$, and changing values for Fr and ϵ; and (b) $c_P = 0.45$, $Fr = 0.01$, $\epsilon = 0.5\%$, and changing values for η. These plots assume the worst-case scenario, where the hydrokinetic turbine is positioned directly downstream of the dam, experiencing the maximum water level increase (i.e., no water surface recovery).

4.1. Net power production

We first look at the net power generation assuming the worst-case scenario, where the CEC is located directly downstream of the dam (i.e., without accounting for any water surface recovery from the CEC backwater rise). Fig. 5a shows the resulting ratio of CEC power gain to hydropower loss ($P_{CEC}/\Delta P_H$) calculated by simultaneously solving Eq. (15) while fixing the power coefficient c_P to 45% and varying the blockage ratio and Froude number within the ranges used in Fig. 3. A typical total hydropower turbine efficiency of 85% ($\eta = 0.85$) was assumed. The ratio appeared to be always less than one, suggesting that, given the specified parameters and simplifications, implementing CEC right downstream of a dam would lead to a greater loss in hydropower output compared to the power produced by the CEC itself.

Notably, the maximum power ratio achievable occurs for low values of blockage ratio and Froude number (i.e., conditions where Eq. (7) is more valid), and is approximately 0.78 for the selected CEC turbine power coefficient and hydropower efficiency. As the Froude number and blockage ratio increase, the ratio between the hydrokinetic gain and hydropower loss decreases. This result suggests that despite an increase in CEC production resulting from either a faster flow (i.e., increasing Fr) or larger/more devices (i.e., increasing ϵ), the hydrokinetic production from a CEC installed directly downstream of a dam can never compensate for the resulting loss in hydraulic head.

Although the power ratio is related to the Froude number, blockage ratio, and CEC efficiency in a more ambiguous way (these independent variables appear in both Eqs. (13) and (14)), its relation with the hydropower efficiency is straightforward and only affects hydropower production. In fact, Eq. (15) shows that if the efficiency of the hydropower turbine decreases, the ratio between hydrokinetic gain and hydropower loss increases. In an idealistic case in which the hydropower turbine achieves perfect efficiency 100% (i.e., $\eta = 1$), the maximum achievable power ratio tends to 0.667 (i.e., 2/3) for very low blockage ratios and Froude numbers, as shown in Fig. 5b. This value is likely related to the assumption of Eq. (7) in which the ratio between the hydrokinetic power production and the total power dissipated in the flow tends to 2/3 for ϵ approaching zero. In this regard, since η influences only the upstream plant, Fig. 5b shows that the maximum ratio between the CEC production and hydropower loss could become greater than 1 for hydropower efficiency lower than 67% (i.e., $\eta = 0.667$) for small blockage and Froude values. Such a low efficiency value however is not common for modern hydropower turbines, and a very low Froude number and blockage ratio is not likely in practical applications for highly efficient hydropower plants. Nevertheless, hydrokinetic development in tailraces might become a viable solution at old sites where the overall efficiency of the hydropower plant has decreased over time, and a full refurbishment might be structurally challenging and economically less convenient.

To install hydrokinetic turbines within the tailrace channel of hydropower plants with more typically high efficiency, the available hydraulic head must preserved. Therefore, it is paramount to optimize the siting location for the CECs to ensure a net positive power generation from the combined CEC–hydropower system while remaining within the tailrace boundaries.

4.2. Siting location: the turbine factors

To study how different parameters affect the net power generation from the system according to different CEC deployment locations, we again set $c_P = 0.45$ and use the typical value of hydropower efficiency, $\eta = 0.85$, as discussed in Section 4.1. We then fix the Froude number (i.e., fixed slope) and change the blockage ratios as $\epsilon = 5\%$, 10%, 15%, and 20%, which fall within the range used for the sensitivity analysis in Section 3.2 and are consistent with the assumption in Eq. (7). As shown in Fig. 6a, the power ratio becomes higher as the siting location of CECs moves further downstream. This shows how deploying CECs further downstream from the dam allows for a recovery of the water surface, thereby mitigating the loss of hydropower and resulting in a higher ratio of energy gain from CECs relative to the loss in hydropower. The optimal location for siting the CECs is determined by the distance at which the water surface returns to its undisturbed level condition. At this juncture, there is no loss of hydraulic head from hydropower generation, thereby enabling pure energy gain from the CECs as the power ratio profile approaches asymptotic ($P_{CEC}/\Delta P_H \to \infty$).

Fig. 6a shows that different blockage ratios have a small effect on the energy ratio profiles. The zoom-in region shown by Fig. 6b further reveals that the increase of blockage ratio will only slightly shift the power ratio profile downward (i.e., a longer distance from the dam is required to locate the CECs to avoid hydropower generation loss). This suggests that increasing deployment of CEC devices (i.e., larger or more devices within a cross-section) will only moderately affect the total power generation and the actual distance from the dam becomes a more relevant parameter. Therefore, a precise siting location can only be determined by evaluating the cost-benefits of increasing turbine installation (dimensions or number) while keeping them within the tailrace channel to capitalize on the benefits of the existing electrical interconnections and the engineered structures. Fig. 6b, can be used as a reference to design the CEC (ϵ) and select the deployment location along with other known parameters (e.g., C_p and η) to ensure a positive power generation ($P_{CEC}/\Delta P_H > 1$) at each specific tailrace channel.

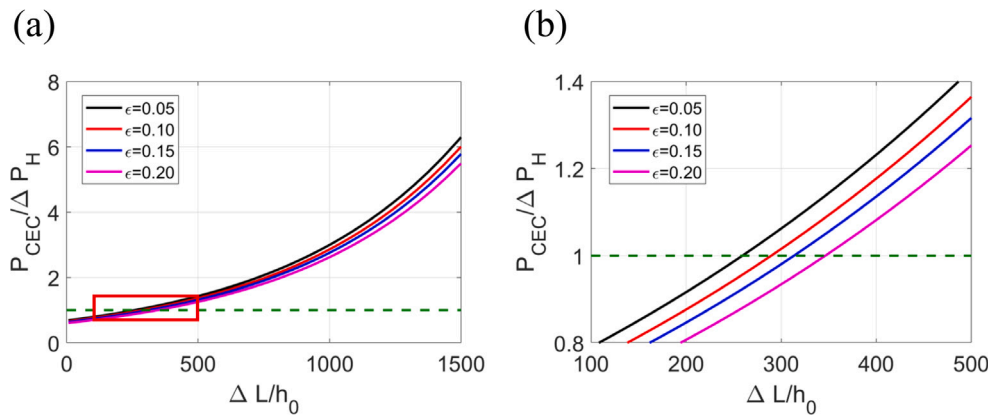

Fig. 6. Power ratio $P_{CEC}/\Delta P_H$ under four different values of $\epsilon = 5\%$, 10%, 15%, and 20% for $c_P = 0.45$, $\eta = 0.85$, and $Fr = 0.3$ (corresponding to $S = 0.0005$) with varying distance from the dam to the CECs siting location normalized by the undisturbed water depth, $\Delta L/h_0$. (b) shows the zoomed-in area indicated by the red box in (a). Dashed green line shows the power ratio $P_{CEC}/\Delta P_H = 1$.

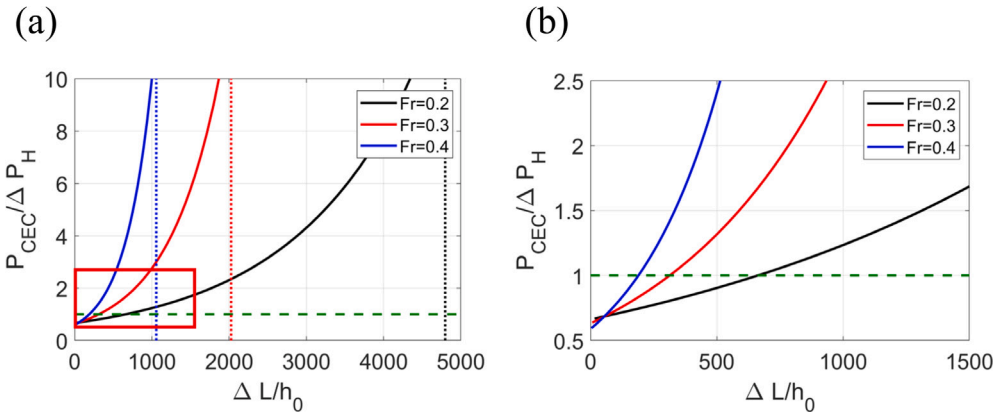

Fig. 7. Power ratio $P_{CEC}/\Delta P_H$ under three different values of $Fr = 0.1$, 0.2, and 0.3 (corresponding to $S = 0.0002 - 0.0008$) for $c_P = 0.45$, $\eta = 0.85$, and $\epsilon = 15\%$ with varying distance from the dam to the CECs siting location normalized by the undisturbed water depth, $\Delta L/h_0$. (b) shows the zoomed-in area indicated by the red box in (a). The dashed green line shows the power ratio $P_{CEC}/\Delta P_H = 1$. The dotted lines in (a) show the asymptotic lines where $\Delta P_H = 0$ (i.e. $\Delta h = 0$).

4.3. Siting location: the hydraulic factors

Different Froude numbers ($Fr = 0.2$, 0.3, and 0.4 with a fixed $\epsilon = 15\%$) reveal a more dramatic change of the power ratio profiles, as compared to changing blockage ratio. Fig. 7a shows that when the Froude number increases (i.e. increase of the channel bottom slope), the water surface profile requires a shorter distance to recover back to undisturbed conditions at the dam. Therefore, higher Froude numbers lead to shorter distances required to reduce the hydropower losses to zero, as indicated by the dotted asymptotic lines (i.e., $\Delta L/h_0 \approx 4800$ for $Fr = 0.2$; $\Delta L/h_0 \approx 2000$ for $Fr = 0.3$; and $\Delta L/h_0 \approx 1000$ for $Fr = 0.4$). Although high Froude numbers (i.e., steeper channel slopes) lead to higher maximum water level increases due to higher drags exerted by the CEC devices, they also reduce the distances required to reach positive net power generation for the combined system, as shown in the zoom-in region in Fig. 7b. This, again, occurs because stronger flow inertia over a steep slope has a stronger ability to restore the water profile back to its equilibrium state once disturbed.

Therefore, we can conclude that tailrace channels with steeper slopes are preferable as CECs could be installed at shorter distances downstream of the dams to reach a positive net power production or even higher efficiency by the CEC–hydropower combined system. This again would potentially drive down installation and maintenance costs by capitalizing on the existing infrastructure.

5. U.S. potential and case studies

5.1. Potential tailrace power generations at major hydropower dams in the United States

Accurate estimates of hydrokinetic energy potentials at hydropower tailraces in the U.S. require information pertaining to the flow and the geometry of these channels. However, detailed data describing tailrace characteristics are not available on a national scale. Therefore, to provide a high-level estimate of the hydrokinetic potential available in tailraces, a subset of sites from the U.S. hydropower fleet with flow information downstream of the dam were analyzed. Historical daily flow records from the USGS Surface Water Database for the Nation [89], were obtained for hydropower facilities across the U.S. using HILARRI [90], a database that links datasets of hydropower dams and power plants, and inland water bodies.

Detailed data processing procedures are described as follows. First, HILARRI was screened to select only sites with dam structures and operational power plants. The locations of these sites were then matched to gauges from the USGS database, limiting to a search distance of 2 km downstream of the dam and records with at least 10 years of data between 1970–2020. This filtering process resulted in 102 hydropower dams/plants with daily flow data that was assumed to be representative of flow in the tailrace channel (i.e., all other inflows that might exist between the dam and stream gauge are ignored). While the flow information can be obtained for a few sites through stream gauge

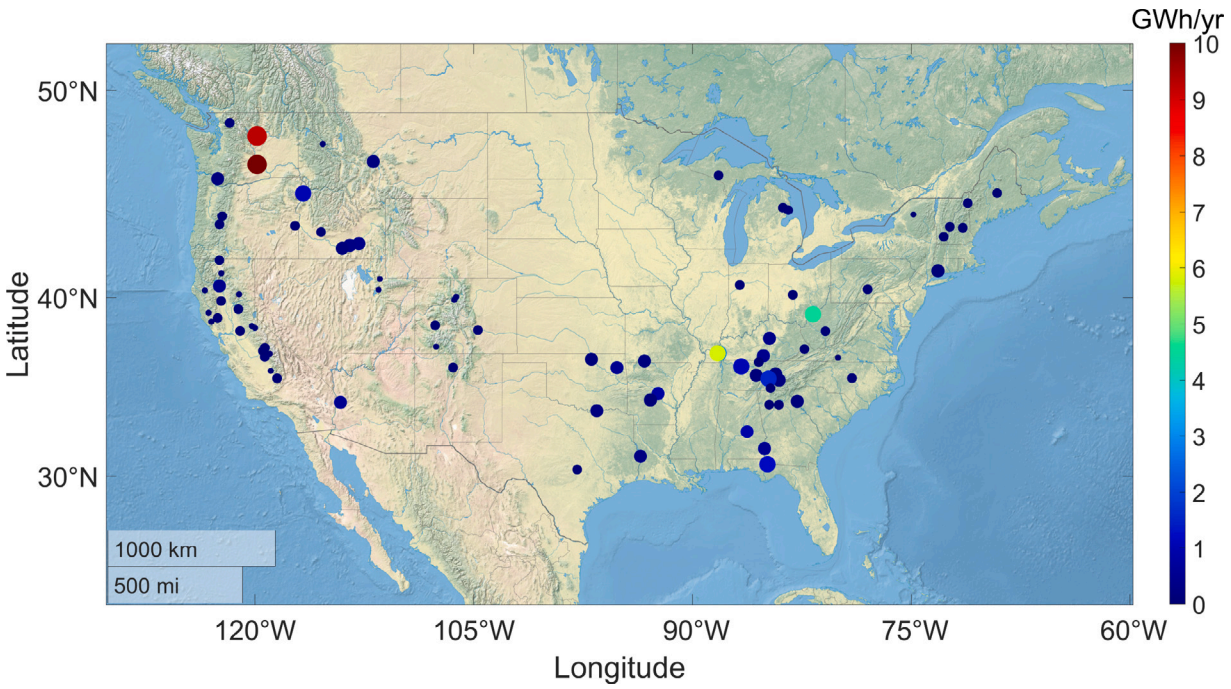

Fig. 8. Spatial distribution of theoretical tailrace hydrokinetic energy potential for an average year in the U.S. main territory (excluding Alaska, Hawai, Puerto Rico, and other Caribbean and Pacific islands) using Eq. (16) for an empirical relation between the discharge, Q, and the channel cross-section, A, proposed by Castro and Jackson [91].

records, physical characteristics (i.e., dimensions) of tailrace channels are not documented in national datasets. Therefore, an empirical power relation between the discharge Q and the channel cross-section area A was used as derived by Castro and Jackson [91], who analyzed field data from hundreds of rivers in the Pacific Northwest:

$$A = 0.58Q^{0.86} \tag{16}$$

Assuming that the CEC devices are constantly running for 24 h a day, we thus estimated the theoretical daily power potential of a single cross-section of these tailrace channels using Eq. (14). For this theoretical assessment, we considered a blockage ratio (ϵ) of 20% and a CEC device power coefficient (c_P) of 0.45, consistent with the CEC parameter configuration detailed in Section 4. We also assume that hydrokinetic turbines are deployed sufficiently downstream to avoid any hydropower losses, thus focusing solely on the hydrokinetic gain. By summing the daily power values for each year, multiplying by 24 h, and calculating the average across the entire data record period from 1970 to 2020, we then derived the mean theoretical energy generation in an average year. Fig. 8 shows the estimated tailrace hydrokinetic energy production at the selected powered dams in the U.S. main territory (excluding Alaska, Hawaii, Puerto Rico, and other Caribbean and Pacific islands). The theoretical energy production is in a range of 1 to 10 GWh/yr for each power dam's tailrace. Although major productions are located in the Pacific Northwest and Southeast regions, all tailrace channel locations herein could provide a total of more than 44.7 GWh/yr across the U.S.

However, the empirical relation between Q and A proposed by Castro and Jackson [91] is sensitive and not accurate everywhere as it was developed using data from rivers located in the Pacific Northwest only. For a more universal relation, we turn to use the empirical formula proposed by Ridgill et al. [12] from a global perspective, which suggests that the mean flow velocity, $V = 0.5Q^{0.2}$, which can be used to estimate the channel cross-section as:

$$A = \frac{Q}{V} = 2Q^{0.8} \tag{17}$$

This leads to a power-law coefficient that is similar to Eq. (16) but with a different leading polynomial coefficient. Fig. 9 shows similar results with slightly different estimated values of power by each tailrace channel, yielding a lower estimated value of the total energy production of 36.3 GWh/yr across the United States for an avearage year.

This analysis does not consider the cut-in threshold velocity required for a CEC device to initiate power generation [73]. Thus, our estimation may overestimate the total power production for our specific assumptions. However, it is important to note that this estimation is limited to a single cross-section of the tailrace, with an assumed fixed blockage ratio, and does not consider the entire length of the tailrace. Consequently, the hydrokinetic potential presented here is actually underestimated and provides only a partial view of the overall resource, considering only one single row of turbines downstream. To perform a comprehensive theoretical assessment, the method proposed by Ridgill et al. [12] should be adopted. In this study, hydrokinetic power is estimated as the direct rate of kinetic energy transfer, using power-law relationships for channel shape and flow velocity as a function of flow rate. However, this model requires knowledge of channel length, which, as previously mentioned, is not publicly available for the U.S. hydropower fleet on a national scale. Therefore, to achieve a complete and accurate estimation of hydrokinetic resources at tailraces, it is crucial to gather more data on channel characteristics and incorporate turbine manufacturing specifications. Additionally, as discussed in Section 4, further information on site-specific features, such as channel slope, geometry, and bottom roughness, is necessary to optimize CEC siting locations and ensure positive net power generation.

Considering the large number of hydropower sites and the lack of required information and direct measurements, a thorough evaluation of the potential can only be conducted in few exploratory locations for now. In Section 5.2, we use existing measurement and modeling data at two exemplary sites together with the proposed 1D analytical model in Section 2 to envision an actual deployment and provide hydrokinetic generation estimates against different siting locations.

5.2. Examples of hydropower sites for CEC deployment

The Wanapum [92] and Priest Rapids [93] hydropower dams are selected as two example sites from the U.S. hydropower fleet to identify potential case studies where our model, in tandem with additional preliminary assessments, can be applied to evaluate potential field

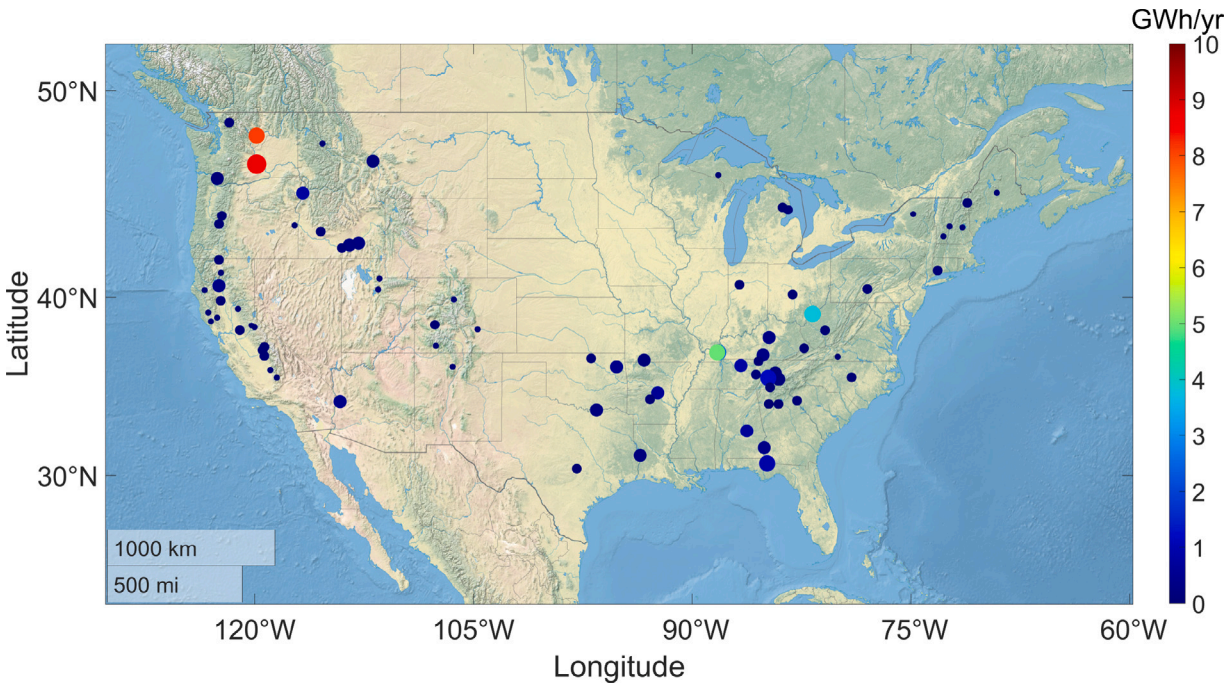

Fig. 9. Spatial distribution of theoretical tailrace hydrokinetic energy potential for an average year in the U.S. main territory (excluding Alaska, Hawai, Puerto Rico, and other Caribbean and Pacific islands) using Eq. (17) with an empirical relation between the discharge, Q, and the channel cross-section, A, proposed by Ridgill et al. [12].

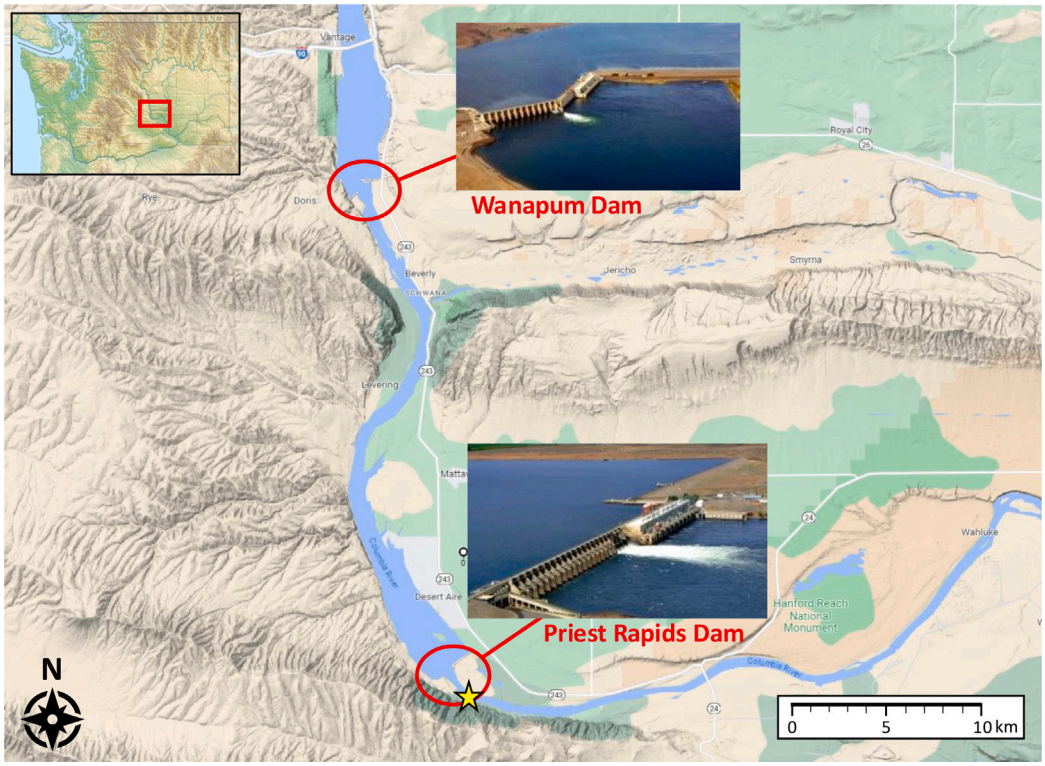

Fig. 10. Locations of the Wanapum Dam (upper inset) and Priest Rapids Dam (lower inset) along the Columbia River. The map is adapted from Google Earth [94]. The inset images are from the Foundation for Water & Energy Education (FWEE) [95].

demonstration projects. The two dams are located approximately 650 kilometers inland from the Pacific Ocean along the Columbia River (see Fig. 10). These two facilities were built under the Priest Rapids Project, providing a combined power capacity of 1893 MW, which ranks as the fifth largest conventional hydropower system on the Columbia River. The two dams are approximately 30 km apart.

The hydraulic data at a downstream site of each dam shown in Table 2 are assessed from multiple data sources: (1) Grant County PUD, (2) the Iowa Institute of Hydraulic Research (IIHR), and (3) the Columbia River Data Access (DART), which are all summarized by Arango [96].

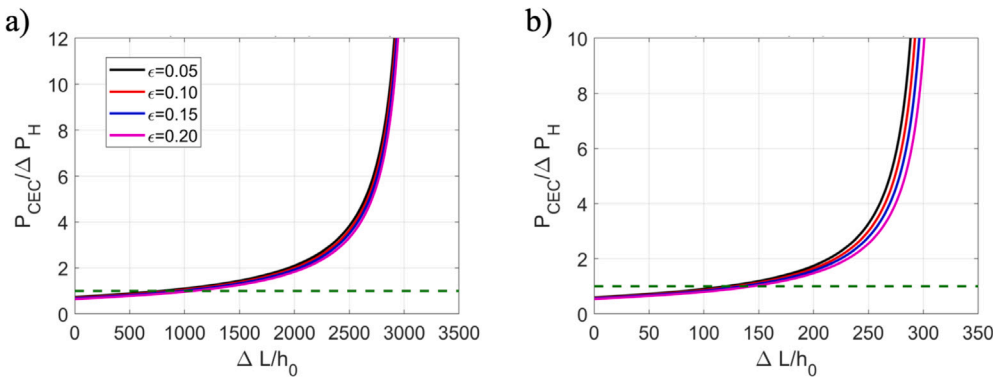

Fig. 11. Net power ratio analysis against varying CEC siting distances from the dam under different blockage ratios, ϵ = 5%, 10%, 15%, and 20% at (a) Wanapum Dam and (b) Priest Rapids Dam along the Columbia River.

Table 2
The averaged integrated hydraulic parameters for a specific cross-section at the downstream site at Wanapum and Priest Rapids dams [96]. The data is based on 50% annual exceedance probability of the total discharge (Q_{50}).

	Wanapum Dam	Priest Rapids Dam
Discharge, Q_{50} (m^3/s)	1410	990
Cross-section area, A_{ch} (m^3)	931.14	284.84
Hydraulic depth, h_0 (m)	9.58	5.81
Mean flow velocity, V_0 (m/s)	1.51	3.49
Froude number, Fr	0.16	0.46
Reynolds number, Re	3.88×10^7	5.24×10^7

Assuming that the 50% annual exceedance probability discharge (i.e., Q_{50}) can fairly represent the equilibrium state discharge where the flow inertia balances with the bottom drag ($S = C_f Fr^2$), we can estimate the mean tailrace slope obtaining $S = 0.00013$ for Wanapum dam and $S = 0.0011$ for Priest Rapids dam. The bottom drag coefficient $C_f \approx 0.005$ is estimated according to Keulegan [97] where $C_f^{-1/2} = \frac{1}{0.41} \ln\left(11\frac{h_0}{k_s}\right)$, and k_s is the channel bottom roughness which is typically 10^{-2} m for a natural-concrete mixed tailrace. Fig. 11 shows the estimations of the power generation ratio under different blockage ratios, ϵ = 5%, 10%, 15%, and 20% by setting $c_P = 0.45$ and $\eta = 0.85$, at both dams. Given the steeper estimated mean slope at Priest Rapids as compared to Wanapum, an ideal CEC tailrace installation would require a relatively shorter distance from the dam structure to obtain a positive net power production as discussed in Section 4.3.

To quantify this, hydropower losses would reduce to zero at Wanapum dam if CEC turbines were installed at a distance ratio of $\Delta L/h_0 \approx 3000$. Considering a tailrace mean water hydraulic depth of $h_0 = 9.58$ m as suggested by the selected downstream cross-section data shown in Table 2, that ratio yields an approximate distance of 28.74 km downstream the dam, which is well beyond the tailrace boundaries and within the Priest Rapids Dam region of influence (see Fig. 10). On the other hand, for Priest Rapids dam, the hydropower losses would reduce to zero at $\Delta L/h_0 \approx 300$, which corresponds to an approximate distance of only 1.74 km from the dam based on the mean water depth of the channel, $h_0 = 5.81$ m. This location, marked by the yellow star in Fig. 10, may be close enough to the dam to still be considered as part of the tailrace channel and thus allow a potential project to capitalize on the existing infrastructure (engineered channel, electrical interconnection, etc.).

Using the hydraulic data and channel dimensions from the Priest Rapids Dam shown in Table 2 for Q_{50}, we can estimate the potential power generation by deploying hydrokinetic turbines at the selected location. Assuming a power coefficient of $c_P = 0.45$ and using the same blockage ratios considered so far (ϵ = 5%, 10%, 15%, and 20%), the expected hydrokinetic power production is approximately 134, 268, 402, and 537 kW, respectively. Based on the channel cross-sectional area indicated in Table 2, $A_{ch} = 284.84 m^2$, these blockage ratios correspond to turbines with a frontal area of $A_T \approx 14$, 28, 43, and 57 m^2 and a diameter of $D_T \approx 4.3$, 6, 7.4, and 8.5 m. However, the few examples of axial-flow turbines currently considered in the U.S. have diameters that do not exceed 5 m, and any other diameters in the list greater than $D_T = 4.3$ would exceed the water depth considered. Therefore, the four blockage ratios used in this example would alternatively correspond to a deployment of 1, 2, 3, and 4 turbines in a single row, each with a nominal diameter of $D_T = 4.3$ m. In this case, the estimated ideal deployment location, where pure hydrokinetic production could be achieved with zero hydropower losses (i.e., at 1.74 km), would be equivalent to 405 times the rotor diameter.

The above estimation combined with the existing data of these two example sites demonstrates how the proposed analytical model can be used to identify potential case studies for future field-scale tests to envision an actual deployment. However, the analysis herein is only a rough estimation based on simplified assumptions. Field measurements and more detailed analyses are needed to evaluate the true feasibility of field applications.

6. Discussion and conclusions

This study presents an initial assessment of the backwater effect resulting from CEC turbine deployment within a single cross-section of a hydropower tailrace channel in subcritical hydraulic conditions ($Fr < 1$). Results are based on a simplified 1D momentum balance approach to estimate the water level increase of the CEC installment as a function of flow hydraulic parameters (i.e., Froude number, bottom slope) and turbine parameters (i.e., blockage ratio, CEC efficiency, and CEC siting location). Within the range of input parameters considered, the estimated water level increase was minimal (under 1%), suggesting small hydropower losses. However, the analysis indicated that, based on the assumptions, these losses would not have been compensated by CEC power production if turbines had been installed too close to the upstream dam. Hydropower losses can be avoided by installing the hydrokinetic devices sufficiently downstream to allow the backwater to recover to the upstream undisturbed level (according to the M1 profile in gradually varied open-channel flows). To determine the optimal CEC location to minimize the head loss, we combined the open-channel backwater equation with the estimated backwater rise to investigate the recovery profile of the water surface level. The power production ratio between the power gain by CECs and the hydropower loss is calculated to study how different parameters (i.e., Froude number and blockage ratio) affect the net power generation from the CEC–hydropower combined system according to different CEC locations.

Our analysis shows that Froude number and blockage ratios are the two most sensitive parameters for the water surface increase and the net power generation. Different blockage ratios will slightly shift the power

ratio profile (CEC energy gain divided by the hydropower loss) downward, suggesting that implementing larger or more CEC devices would require a longer distance from the dam to locate the CECs in order to reduce the hydropower generation loss. On the other hand, changes in the Froude number, which is linked to the channel slope of the tailrace channel, have an even greater impact on the power ratio, resulting in totally different profiles. Higher Froude numbers (i.e., steeper channel slopes) lead to higher water level increases caused by a stronger drag exerted from CECs, which in turn lead to lower initial power ratios. However, because of stronger flow inertia, the system recovers faster to its undisturbed state implying that CECs can be installed closer to the dam while still reaching positive power generation. This suggests that steeper tailrace channels with higher Froude numbers may be more suitable for developing a CEC–hydropower combined system.

An overview of potential CEC deployment in tailrace channels is presented by showing high-level estimations of potential hydrokinetic energy production at 102 dams from the U.S. hydropower fleet. Although limited to a relatively small number of dams, this analysis showed that a total of 36.3 GWh/yr of theoretical production could be added across the U.S. However, this value is likely underestimated, as it considers only a single cross-section (i.e., it does not account for the entire tailrace length) and assumes a fixed blockage ratio. Finally, two tailrace sites located in the Pacific Northwest were selected for a more comprehensive analysis based on the proposed 1D model. Given the limitation of the present work to an analytical analysis, more rigorous modeling approaches would need to be implemented for a more precise quantification. Our results also suggest that additional data and field measurements of channel characteristics are needed to better predict the best CEC siting location for efficient CEC–hydropower systems designs.

Future research should introduce more thorough analysis (e.g., detailed analytical or numerical modeling) that could further investigate CEC tailrace application feasibility by incorporating solutions with less simplifying assumptions and more comprehensive solutions for Eq. (7) [75]. The analysis should also be extended to the deployment of CEC arrays with multiple rows to understand the cumulative effect of multiple turbines on the backwater effect. Further modifications can improve the proposed model for more general and more complex channel shapes that are common for other tailrace channels.

In conclusion, hydropower tailrace channels offer an attractive source of hydrokinetic energy within a controlled, engineered system that is in close proximity to existing power grid interconnection infrastructure. This project provides a better understanding of the detrimental effect (hydropower loss), the benefit (extra energy production), and the solution (optimized siting location) of tailrace applications, and it unveils sites where further tangible analysis could be pursued. The results support the idea of hydrokinetic energy harnessing in hydro tailrace channels, which can initiate future research and investigations along with the ongoing advancements in the hydrokinetic energy industry to improve CEC tailrace application feasibility. Looking at this application from a different perspective, tailrace channels could also offer an interesting opportunity for full-scale testing of hydrokinetic turbines. Dams across the U.S. could be used as test facilities where technology developers and researchers could install their devices within a highly engineered channel with well-defined boundary conditions and existing grid interconnection access, while also producing tangible revenue that could mitigate the economical investment for testing. However, CEC tailrace applications present several additional challenges that must be addressed (including energy, economic, and environmental challenges; design considerations; and stakeholder acceptance), which could limit their practicality and make deployment infeasible. Future studies should address these considerations while rigorous and site-specific cost–benefit analysis should be implemented to evaluate feasibility.

CRediT authorship contribution statement

Chien-Yung Tseng: Writing – review & editing, Writing – original draft, Visualization, Investigation, Formal analysis, Data curation. **Mirko Musa:** Writing – review & editing, Writing – original draft, Validation, Supervision, Project administration, Methodology, Investigation, Funding acquisition, Formal analysis, Data curation, Conceptualization.

Declaration of competing interest

The authors declare that they have no known competing financial interests or personal relationships that could have appeared to influence the work reported in this paper.

Acknowledgments

The authors would like to thank Dr. Carly Hansen for providing the data used to estimate the hydrokinetic potential at select hydropower dams across the United States, and to Kevin Stewart and Scott DeNeale for their insightful input and review of an early draft of the manuscript.

The project was supported by the US Department of Energy's Water Power Technologies Office (WPTO). This manuscript has been authored by UT-Battelle, LLC, under contract DE-AC05-00OR22725 with the US Department of Energy (DOE). The US government retains and the publisher, by accepting the article for publication, acknowledges that the US government retains a nonexclusive, paid-up, irrevocable, worldwide license to publish or reproduce the published form of this manuscript or allow others to do so, for US government purposes. DOE will provide public access to these results of federally sponsored research in accordance with the DOE Public Access Plan (http://energy.gov/downloads/doe-public-access-plan).

Data availability

Some or all data, models, or code that support the findings of this study are available from the corresponding author upon reasonable request.

References

[1] US Energy Information Administration (EIA), Wind has surpassed hydro as most-used renewable electricity generation source in U.S., 2020, https://www.eia.gov/todayinenergy/detail.php?id=42955. (Accessed 09 February 2024).
[2] US Energy Information Administration (EIA), In the first half of 2022, 24 from renewable sources, 2022, https://www.eia.gov/todayinenergy/detail.php?id=53779. (Accessed 09 February 2024).
[3] United Nations (UN), COP28 ends with call to 'transition away' from fossil fuels; UN's Guterres says phaseout is inevitable, 2023, https://news.un.org/en/story/2023/12/1144742. (Accessed 09 February 2024).
[4] US Energy Information Administration (EIA), Renewable generation surpassed coal and nuclear in the U.S. electric power sector in 2022, 2023, https://www.eia.gov/todayinenergy/detail.php?id=55960. (Accessed 09 February 2024).
[5] US Energy Information Administration (EIA), In the first half of 2022, 24% of U.S. electricity generation came from renewable sources, 2023, https://www.eia.gov/tools/faqs/faq.php?id=427&t=4. (Accessed 09 February 2024).
[6] S.C. James, E.L. Johnson, J. Barco, J.D. Roberts, Simulating current-energy converters: SNL-EFDC model development, verification, and parameter estimation, Renew. Energy 147 (2020) 2531–2541.
[7] W. Ibrahim, M. Mohamed, R. Ismail, P. Leung, W. Xing, A. Shah, Hydrokinetic energy harnessing technologies: A review, Energy Rep. 7 (2021).
[8] E. Browning, S. Olson, R. Fao, A. Keester, J. McVey, Tanana river test site model verification using the marine and hydrokinetic toolkit (MHKiT), Energies 16 (8) (2023) 3326.
[9] T.A. Adcock, S. Draper, R.H. Willden, C.R. Vogel, The fluid mechanics of tidal stream energy conversion, Annu. Rev. Fluid Mech. 53 (2021) 287–310.
[10] L. Kilcher, M. Fogarty, M. Lawson, Marine Energy in the United States: An Overview of Opportunities, Tech. Rep. NREL/TP-5700-78773, National Renewable Energy Lab (NREL), Golden, CO, 2021, URL https://www.nrel.gov/docs/fy21osti/78773.pdf.

[11] M. Ridgill, S.P. Neill, M.J. Lewis, P.E. Robins, S.D. Patil, Global riverine theoretical hydrokinetic resource assessment, Renew. Energy 174 (2021) 654–665.
[12] M. Ridgill, M.J. Lewis, P.E. Robins, S.D. Patil, S.P. Neill, Hydrokinetic energy conversion: A global riverine perspective, J. Renew. Sustain. Energy 14 (4) (2022).
[13] Y.L. Young, M.R. Motley, R. Barber, E.J. Chae, N. Garg, Adaptive composite marine propulsors and turbines: progress and challenges, Appl. Mech. Rev. 68 (6) (2016) 060803.
[14] G.S. Payne, T. Stallard, R. Martinez, Design and manufacture of a bed supported tidal turbine model for blade and shaft load measurement in turbulent flow and waves, Renew. Energy 107 (2017) 312–326, http://dx.doi.org/10.1016/j.renene.2017.01.068, URL https://linkinghub.elsevier.com/retrieve/pii/S0960148117300782.
[15] D. Apsley, P. Stansby, Fluctuating loads on a tidal turbine due to velocity shear and turbulence: Comparison of CFD with field data, Renew. Energy 112 (2017) 235–246.
[16] E.E. Lust, K.A. Flack, L. Luznik, Survey of the near wake of an axial-flow hydrokinetic turbine in the presence of waves, Renew. Energy 146 (2020) 2199–2209, http://dx.doi.org/10.1016/j.renene.2019.08.067.
[17] P. Ouro, T. Nishino, Performance and wake characteristics of tidal turbines in an infinitely large array, J. Fluid Mech. 925 (2021) A30.
[18] P.K. Modali, A. Vinod, A. Banerjee, Towards a better understanding of yawed turbine wake for efficient wake steering in tidal arrays, Renew. Energy 177 (2021) 482–494.
[19] S. Chawdhary, D. Angelidis, J. Colby, D. Corren, L. Shen, F. Sotiropoulos, Multiresolution large-eddy simulation of an array of hydrokinetic turbines in a field-scale river: The roosevelt island tidal energy project in New York City, Water Resour. Res. 54 (12) (2018) 10,188–10,204, http://dx.doi.org/10.1029/2018WR023345, arXiv:1810.03228.
[20] M. Nuernberg, L. Tao, Experimental study of wake characteristics in tidal turbine arrays, Renew. Energy 127 (2018) 168–181.
[21] C.M. Niebuhr, M. van Dijk, V.S. Neary, J.N. Bhagwan, A review of hydrokinetic turbines and enhancement techniques for canal installations: Technology, applicability and potential, in: Renewable and Sustainable Energy Reviews, vol. 113, 2019, 109240, http://dx.doi.org/10.1016/j.rser.2019.06.047, URL https://linkinghub.elsevier.com/retrieve/pii/S136403211930440X.
[22] M. Musa, C. Hill, M. Guala, Interaction between hydrokinetic turbine wakes and sediment dynamics: array performance and geomorphic effects under different siting strategies and sediment transport conditions, Renew. Energy 138 (2019) 738–753.
[23] M. Guerra, A.E. Hay, R. Karsten, G. Trowse, R.A. Cheel, Turbulent flow mapping in a high-flow tidal channel using mobile acoustic Doppler current profilers, Renew. Energy 177 (2021) 759–772.
[24] A. Bharath, H. Ross, C. Nichols, A. Simms, M. Murphy, R. Raye, P. O'Byrne, M. Monahan, M. Wosnik, Open water blade strain measurements on a vertical-axis tidal turbine, in: International Conference on Offshore Mechanics and Arctic Engineering, Vol. 86908, American Society of Mechanical Engineers, 2023, V008T09A003.
[25] M. Musa, C. Hill, F. Sotiropoulos, M. Guala, Performance and resilience of hydrokinetic turbine arrays under large migrating fluvial bedforms, Nature Energy 3 (10) (2018) 839–846, http://dx.doi.org/10.1038/s41560-018-0218-9.
[26] K. Kirby, S. Ferguson, C. Rennie, I. Nistor, J. Cousineau, Assessments of available riverine hydrokinetic energy: A review, Can. J. Civil Eng. 49 (6) (2022) 839–854.
[27] J.L. Gutenson, K.A. Staebell, M.D. Wahl, A.C. Petri, M.P. Duczynski, A practical evaluation of micro-hydrokinetic power potential for the continental United States, J. Hydrol. Reg. Stud. 47 (2023) 101402.
[28] B. Kirke, Towards more cost-effective river hydrokinetic turbines, Energy Sustain. Dev. 78 (2024) 101370.
[29] Emrgy Inc, Unleashing water's natural power, 2024, https://emrgy.com/. (Accessed 12 February 2024).
[30] Ocean Renewable Power Company (ORPC), Case Study - Igiugig, Alaska, 2024, https://orpc.co/case-study/. (Accessed 12 February 2024).
[31] Department of Energy (DOE), Biden-Harris Administration Invests Nearly $16 Million to Advance Marine Energy in the U.S., 2024, https://www.energy.gov/articles/biden-harris-administration-invests-nearly-16-million-advance-marine-energy-us-1. (Accessed 12 February 2024).
[32] K.W. Tan, B. Kirke, M. Anyi, Small-scale hydrokinetic turbines for remote community electrification, Energy Sustain. Dev. 63 (2021) 41–50.
[33] E.J. Brown, A.L. King, P.X. Duvoy, E. Trochim, J.L. Kasper, M.L. Wilson, T.M. Ravens, Site suitability analysis of hydrokinetic river energy resources at community microgrids on the Kuskokwim River, Alaska, Renew. Energy 217 (2023) 119083.
[34] A. MacMillan, K.R. Schell, C. Roughley, A predictive model of velocity for local hydrokinetic power assessment based on remote sensing data, Renew. Energy 211 (2023) 285–295.
[35] I.F.S. dos Santos, R.G.R. Camacho, G.L. Tiago Filho, A.C.B. Botan, B.A. Vinent, Energy potential and economic analysis of hydrokinetic turbines implementation in rivers: An approach using numerical predictions (CFD) and experimental data, Renew. Energy 143 (2019) 648–662.
[36] E. Quaranta, S. Muntean, Wasted and excess energy in the hydropower sector: A European assessment of tailrace hydrokinetic potential, degassing-methane capture and waste-heat recovery, Appl. Energy 329 (2023) 120213.
[37] E. Quaranta, Stream water wheels as renewable energy supply in flowing water: Theoretical considerations, performance assessment and design recommendations, Energy Sustain. Dev. 45 (2018) 96–109, http://dx.doi.org/10.1016/j.esd.2018.05.002, URL https://linkinghub.elsevier.com/retrieve/pii/S0973082618301704.
[38] E. Lalander, M. Leijon, In-stream energy converters in a river – Effects on upstream hydropower station, Renew. Energy 36 (1) (2011) 399–404, http://dx.doi.org/10.1016/j.renene.2010.05.019, URL https://linkinghub.elsevier.com/retrieve/pii/S0960148110002533.
[39] Y. Liu, D.J. Packey, Combined-cycle hydropower systems - The potential of applying hydrokinetic turbines in the tailwaters of existing conventional hydropower stations, Renew. Energy 66 (2014) 228–231, http://dx.doi.org/10.1016/j.renene.2013.12.007.
[40] R.D.M. Ramírez, F.I. Cuervo, C.A.M. Rico, Technical and financial valuation of hydrokinetic power in the discharge channels of large hydropower plants in Colombia: A case study, Renew. Energy 99 (2016) 136–147.
[41] P. da Silva Holanda, C.J.C. Blanco, A.L.A. Mesquita, A.C.P.B. Junior, N.M. de Figueiredo, E.N. Macêdo, Y. Secretan, Assessment of hydrokinetic energy resources downstream of hydropower plants, Renew. Energy 101 (2017) 1203–1214.
[42] L.L. Ladokun, B.F. Sule, K.R. Ajao, A.G. Adeogun, Resource assessment and feasibility study for the generation of hydrokinetic power in the tailwaters of selected hydropower stations in Nigeria, Water Sci. 32 (2) (2018) 338–354.
[43] M. Kartezhnikova, T.M. Ravens, Hydraulic impacts of hydrokinetic devices, Renew. Energy 66 (2014) 425–432, http://dx.doi.org/10.1016/j.renene.2013.12.034.
[44] C.M. Niebuhr, C. Hill, M. Van Dijk, L. Smith, Development of a hydrokinetic turbine backwater prediction model for inland flow through validated CFD models, Processes 10 (7) (2022) 1310.
[45] L. Cacciali, L. Battisti, S. Dell'Anna, Multi-array design for hydrokinetic turbines in hydropower canals, Energies 16 (5) (2023) 2279.
[46] L. Cacciali, L. Battisti, S. Dell'Anna, Backwater assessment for the energy conversion through hydrokinetic turbines in subcritical prismatic canals, Ocean Eng. 267 (2023) 113246.
[47] R.J. Stevens, C. Meneveau, Flow structure and turbulence in wind farms, Annu. Rev. Fluid Mech. 49 (1) (2017) 311–339.
[48] F. Porté-Agel, M. Bastankhah, S. Shamsoddin, Wind-turbine and wind-farm flows: a review, Bound.-Layer Meteorol. 174 (1) (2020) 1–59.
[49] J. Hong, M. Toloui, L.P. Chamorro, M. Guala, K. Howard, S. Riley, J. Tucker, F. Sotiropoulos, Natural snowfall reveals large-scale flow structures in the wake of a 2.5-MW wind turbine, Nature Commun. 5 (1) (2014) 4216.
[50] X. Yang, F. Sotiropoulos, A new class of actuator surface models for wind turbines, Wind Energy 21 (5) (2018) 285–302.
[51] D. Foti, X. Yang, M. Guala, F. Sotiropoulos, Wake meandering statistics of a model wind turbine: Insights gained by large eddy simulations, Phys. Rev. Fluids 1 (4) (2016) 044407.
[52] B. Dou, M. Guala, L. Lei, P. Zeng, Experimental investigation of the performance and wake effect of a small-scale wind turbine in a wind tunnel, Energy 166 (2019) 819–833.
[53] L. Myers, A. Bahaj, Wake studies of a 1/30th scale horizontal axis marine current turbine, Ocean Eng. 34 (5–6) (2007) 758–762.
[54] L. Chamorro, C. Hill, S. Morton, C. Ellis, R. Arndt, F. Sotiropoulos, On the interaction between a turbulent open channel flow and an axial-flow turbine, J. Fluid Mech. 716 (2013) 658–670.
[55] S. Tedds, I. Owen, R. Poole, Near-wake characteristics of a model horizontal axis tidal stream turbine, Renew. Energy 63 (2014) 222–235.
[56] T. Stallard, T. Feng, P. Stansby, Experimental study of the mean wake of a tidal stream rotor in a shallow turbulent flow, J. Fluids Struct. 54 (2015) 235–246.
[57] Y. Chen, B. Lin, J. Lin, S. Wang, Experimental study of wake structure behind a horizontal axis tidal stream turbine, Appl. Energy 196 (2017) 82–96.
[58] E.E. Lust, K.A. Flack, L. Luznik, Survey of the near wake of an axial-flow hydrokinetic turbine in quiescent conditions, Renew. Energy 129 (2018) 92–101.
[59] S. Kang, X. Yang, F. Sotiropoulos, On the onset of wake meandering for an axial flow turbine in a turbulent open channel flow, J. Fluid Mech. 744 (2014) 376–403.
[60] S. Chawdhary, C. Hill, X. Yang, M. Guala, D. Corren, J.A. Colby, F. Sotiropoulos, Wake characteristics of a TriFrame of axial-flow hydrokinetic turbines, Renew. Energy 109 (2017) 332–345, http://dx.doi.org/10.1016/j.renene.2017.03.029.
[61] P. Ouro, L. Ramírez, M. Harrold, Analysis of array spacing on tidal stream turbine farm performance using Large-Eddy Simulation, J. Fluids Struct. 91 (2019) 102732.
[62] J. Sandoval, K. Soto-Rivas, C. Gotelli, C. Escauriaza, Modeling the wake dynamics of a marine hydrokinetic turbine using different actuator representations, Ocean Eng. 222 (2021) 108584.
[63] A. Posa, R. Broglia, Momentum recovery downstream of an axial-flow hydrokinetic turbine, Renew. Energy 170 (2021) 1275–1291.

[64] Z. Zhang, F. Sotiropoulos, A. Khosronejad, Predicting turbulent wake flow of marine hydrokinetic turbine arrays in large-scale waterways via physics-enhanced convolutional neural networks, Phys. Fluids 36 (4) (2024).
[65] V.G. Nago, I.F.S. dos Santos, M.J. Gbedjinou, J.H.R. Mensah, G.L. Tiago Filho, R.G.R. Camacho, R.M. Barros, A literature review on wake dissipation length of hydrokinetic turbines as a guide for turbine array configuration, Ocean Eng. 259 (2022) 111863.
[66] C.M. Niebuhr, S. Schmidt, M. Van Dijk, L. Smith, V.S. Neary, A review of commercial numerical modelling approaches for axial hydrokinetic turbine wake analysis in channel flow, Renew. Sustain. Energy Rev. 158 (2022) 112151.
[67] C. Manes, M. Brocchini, Local scour around structures and the phenomenology of turbulence, J. Fluid Mech. 779 (2015) 309–324.
[68] G. Gioia, F. Bombardelli, Scaling and similarity in rough channel flows, Phys. Rev. Lett. 88 (1) (2001) 014501.
[69] M. Musa, M. Heisel, M. Guala, Predictive model for local scour downstream of hydrokinetic turbines in erodible channels, Phys. Rev. Fluids 3 (2) (2018) 024606.
[70] Z. Defne, K.A. Haas, H.M. Fritz, Numerical modeling of tidal currents and the effects of power extraction on estuarine hydrodynamics along the Georgia coast, USA, Renew. Energy 36 (12) (2011) 3461–3471.
[71] D. Hasegawa, J. Sheng, D.A. Greenberg, K.R. Thompson, Far-field effects of tidal energy extraction in the Minas Passage on tidal circulation in the Bay of Fundy and Gulf of Maine using a nested-grid coastal circulation model, Ocean Dyn. 61 (2011) 1845–1868.
[72] Z. Yang, T. Wang, A.E. Copping, Modeling tidal stream energy extraction and its effects on transport processes in a tidal channel and bay system using a three-dimensional coastal ocean model, Renew. Energy 50 (2013) 605–613.
[73] M. Lewis, R.O. Murray, S. Fredriksson, J. Maskell, A. de Fockert, S.P. Neill, P.E. Robins, A standardised tidal-stream power curve, optimised for the global resource, Renew. Energy 170 (2021) 1308–1323.
[74] C. Garrett, P. Cummins, The efficiency of a turbine in a tidal channel, J. Fluid Mech. 588 (2007) 243–251, http://dx.doi.org/10.1017/S0022112007007781, URL https://www.cambridge.org/core/services/aop-cambridge-core/content/view/0B669CAB1CC61009F51577A774F3C9DD/S0022112007007781a.pdf/efficiency_of_a_turbine_in_a_tidal_channel.pdf.
[75] B.L. Polagye, Hydrodynamic Effects of Kinetic Power Extraction by in-Stream Tidal Turbines (ProQuest dissertations and theses), 2009, p. 184.
[76] M.I. Yuce, A. Muratoglu, Hydrokinetic energy conversion systems: A technology status review, Renew. Sustain. Energy Rev. 43 (2015) 72–82, http://dx.doi.org/10.1016/j.rser.2014.10.037.
[77] N.D. Laws, B.P. Epps, Hydrokinetic energy conversion: Technology, research, and outlook, Renew. Sustain. Energy Rev. 57 (2016) 1245–1259, http://dx.doi.org/10.1016/j.rser.2015.12.189.
[78] G.J. Arcement, V.R. Schneider, et al., Guide for selecting Manning's roughness coefficients for natural channels and flood plains, vol. 2339, US Government Printing Office Washington, DC, 1989.
[79] C. Hill, M. Musa, L.P. Chamorro, C. Ellis, M. Guala, Local scour around a model hydrokinetic turbine in an erodible channel, J. Hydraul. Eng. 140 (8) (2014) 04014037.
[80] C. Hill, M. Musa, M. Guala, Interaction between instream axial flow hydrokinetic turbines and uni-directional flow bedforms, Renew. Energy 86 (2016) 409–421.
[81] L. Cacciali, L. Battisti, S. Dell'Anna, G. Soraperra, Case study of a cross-flow hydrokinetic turbine in a narrow prismatic canal, Ocean Eng. 234 (2021) 109281.
[82] A. Gharib Yosry, E. Alvarez Alvarez, R. Espina Valdes, A. Pandal, E. Blanco Marigorta, et al., Experimental and multiphase modeling of small vertical-axis hydrokinetic turbine with free-surface variations, Renew. Energy 203 (2023).
[83] B. Gunawan, J. Roberts, V. Neary, Hydrodynamic effects of hydrokinetic turbine deployment in an irrigation canal, in: Proceedings of the 3rd Marine Energy Technology Symposium, Washington, DC, USA, 2015, pp. 27–29.
[84] B. Gunawan, V.S. Neary, J. Mortensen, J. Roberts, Assessing and Testing Hydrokinetic Turbine Performance and Effects on Open Channel Hydrodynamics: An Irrigation Canal Case Study, Tech. Rep., U.S. Department of Energy, 2017, http://dx.doi.org/10.32964/tj16.3.
[85] P. Bachant, M. Wosnik, Characterising the near-wake of a cross-flow turbine, J. Turbulence 16 (4) (2015) 392–410.
[86] B. Strom, S.L. Brunton, B. Polagye, Intracycle angular velocity control of cross-flow turbines, Nature Energy 2 (8) (2017) 1–9.
[87] M.A. Miller, S. Duvvuri, I. Brownstein, M. Lee, J.O. Dabiri, M. Hultmark, Vertical-axis wind turbine experiments at full dynamic similarity, J. Fluid Mech. 844 (2018) 707–720.
[88] C.M. Puertas-Frías, C.S. Willson, P.A. García-Salaberri, Design and economic analysis of a hydrokinetic turbine for household applications, Renew. Energy 199 (2022) 587–598.
[89] US Geological Survey, National Water Information System Data Available on the World Wide Web (USGS Water Data for the Nation), USGS Surface-Water Annual Statistics for Wisconsin, 2016, http://dx.doi.org/10.5066/F7P55KJN, http://waterdata.usgs.gov/nwis/. (Accessed 14 June 2023).
[90] C. Hansen, P. Matson, Hydropower Infrastructure - LAkes, Reservoirs, and RIvers (HILARRI), V2, 2023, http://dx.doi.org/10.21951/HILARRI/1960141, URL https://www.osti.gov/biblio/1960141.
[91] J.M. Castro, P.L. Jackson, Bankfull discharge recurrence intervals and regional hydraulic geometry relationships: patterns in the pacific northwest, USA 1, JAWRA J. Am. Water Resour. Assoc. 37 (5) (2001) 1249–1262.
[92] Columbia Basin Research, Wanapum Dam - Hydroelectric Project Information, 2023, https://www.cbr.washington.edu/dart/hydro/wanapum. (Accessed 21 February 2024).
[93] Columbia Basin Research, Priest Rapids Dam - Hydroelectric Project Information, 2023, https://www.cbr.washington.edu/hydro/priestrapids. (Accessed 21 February 2024).
[94] Google, Google Earth, 2024, This map includes data from Airbus, https://earth.google.com/web. (Accessed 21 February 2024).
[95] Foundation for Water & Energy Education, Priest Rapids: Columbia River, WA, 2024, https://fwee.org/priest-rapids-hydroelectric-project/. (Accessed 21 February 2024).
[96] M.a. Arango, Resource Assessment and Feasibility Study for Use of Hydrokinetic Turbines in the Tailwaters of the Priest Rapids Project (Ph.D. thesis), University of Washington, 2011, p. 158.
[97] G.H. Keulegan, Laws of turbulent flow in open channels, vol. 21, National Bureau of Standards Gaithersburg, MD, 1938.